Complex refractive index of ammonium nitrate in the 2–20-μm spectral range

Maurice A. Jarzembski, Mark L. Norman, Kirk A. Fuller, Vandana Srivastava, and Dean R. Cutten

Using high-resolution Fourier-transform infrared absorbance and transmittance spectral data for ammonium sulfate (AMS), calcium carbonate (CAC), and ammonium nitrate (AMN), we made comparisons with previously published complex refractive-index data for AMS and CAC to infer experimental parameters to determine the imaginary refractive index for AMN in the infrared wavelength range from 2 to 20 μm. Subtractive Kramers–Kronig mathematical relations were applied to calculate the real refractive index for the three compositions. Excellent agreement for AMS and CAC with the published values was found, validating the complex refractive index obtained for AMN. We performed backscatter calculations using a log-normal size distribution for AMS, AMN, and CAC aerosols to show differences in their backscattered spectra.

OCIS codes: 290.3030, 300.0300, 010.0010, 120.4530, 300.6340, 280.0280.

1. Introduction

Atmospheric aerosols can have both a direct and an indirect climatic forcing effect on the thermal budget of the atmosphere,[1,2] depending on how they scatter solar and terrestrial radiation. Their complex refractive index is an important factor in the modeling of their scattering as a function of wavelength. Depending on their composition, aerosols can have varying complex refractive-index values from the visible to the mid-infrared (IR) regions of the electromagnetic spectrum. This is the spectral region for climatic interest where some atmospheric aerosols may have a more dramatic effect than others. Realizing that the complex refractive index of aerosols is such an important atmospheric parameter, the need to know its value as a function of wavelength for the more prevalent and important climatically significant aerosols becomes apparent. Except for water and ice[3] and a few atmospheric aerosols such as sulfuric acid,[4] nitric acid trihydrate,[5] aluminum oxide,[6] sodium chloride,[6] ammonium sulfate,[6,7] and certain dust[7–12] compositions, the complex refractive index of many aerosols found in the atmosphere is not well known in the mid-IR spectral range.

The complex refractive index for aerosol compositions could be determined from several different spectroscopic techniques. Absorbance and transmittance measurements with Fourier-transform infrared (FTIR) spectroscopy is commonly performed, and spectra of many compositions have been measured in various research institutions with this method[13–15] for industrial, technical, or pedagogical reasons. Even though FTIR spectroscopic measurements of many compositions have been made and cataloged, absorbance and transmittance spectra are not, in general, converted to a complex refractive index over the measured wavelength regime; also, key measurement parameters to do so at a later time are also not always available. Furthermore, atmospheric scientists requiring aerosol compositional and complex refractive-index information either for climate or meteorological studies may not have the necessary instrumentation to go from spectral measurements to optical properties. Therefore in this paper we present use of existing high-quality FTIR spectroscopic data to infer necessary but unknown variables from that data to determine the complex

M. A. Jarzembski (maurice.jarzembski@msfc.nasa.gov), K. A. Fuller, V. Srivastava, and D. R. Cutten are with the Global Hydrology and Climate Center, 320 Sparkman Drive, Huntsville, Alabama 35805. When this research was performed, M. A. Jarzembski was with the NASA Marshall Space Flight Center. K. A. Fuller and D. R. Cutten were with the University of Alabama in Huntsville, and V. Srivastava was with the Universities Space Research Association. D. R. Cutten in now retired and V. Srivastava is now with the University of Alabama in Huntsville. When this research was performed, M. L. Norman was with the University of North Carolina. He is now with SensIR Technologies, 15 Great Pasture Road, Danbury, Connecticut 06810.

Received 3 May 2002; revised manuscript received 25 October 2002.

0003-6935/03/060922-09$15.00/0

refractive index of various compositions. Ammonium nitrate (NH_4NO_3) (AMN), ammonium sulfate [$(NH_4)_2SO_4$] (AMS), and calcium carbonate ($CaCO_3$) (CAC) were chosen for the analysis. The complex refractive index for the last two compositions have already been documented[6,16] in the near- to mid-IR spectral region and are used here for comparison. However, the complex refractive index for AMN in the 2–20-μm wavelength, to the best of our knowledge, could not be found in the literature. AMN is of special interest[17–19] because it is considered a significant anthropogenically produced constituent of the atmospheric particulate matter ($PM_{2.5}$) of extreme impact to pollution and climate forcing. In the atmosphere, sulfates and nitrates compete for ammoniation, so where there are less sulfur-based compounds present (e.g., in regions of fewer power plants such as the western United States), then nitrates scavenge the available ammonia, becoming an important aerosol component. The determination of AMN's complex refractive index in this wavelength regime is presented here together with AMS and CAC as reference and subsequent validation of the technique. Obtaining more knowledge of optical properties of important aerosols like AMN leads for better prediction of the aerosol's contribution to climate forcing. Therefore we present a determination of the complex refractive index for AMN as well as a methodology to determine the complex refractive index of other aerosol compositions using already published FTIR spectra.

2. Methodology

Reviewing the literature shows that an extensive compilation of well-documented FTIR spectra for over 10,000 chemical compositions (organic and inorganic) is found in the *Sigma Library of FT-IR Spectra*.[15] The high-resolution spectra are given in terms of absorbance and transmittance as a function of wave number (wavelength) between 4000 cm^{-1} (2.5 μm) and 400 cm^{-1} (25 μm). Many of the spectra are measured in the chemically inert mineral oil Nujol. The published spectra show extremely fine details of the signature characteristic for each substance. However, the spectra were not used for determination of optical properties of the substance. Consequently and unfortunately, concentrations of the chemical compositions in Nujol as well as sample thickness per spectra were not documented in the published text. Had these key parameters been measured and documented, then the imaginary refractive index could be easily determined from the absorbance data that could lead to the real refractive index by use of the subtractive Kramers–Kronig (K–K) mathematical relations.[20,21]

Nonetheless, the spectra cited in the Sigma Library have high resolution, and the spectra in terms of their baseline behavior and absorption line strengths are of high quality. Therefore it is possible with simplified calculation methods to use these spectra to derive an excellent estimation of the complex refractive index for a chemical composition, such as AMN, whose optical properties are not well understood provided that a good comparison could be made with another chemical composition, such as AMS, in the Sigma Library whose complex refractive indices have been more rigorously derived as a function of wavelength. Therefore our procedure in this research is to use the measured absorbance and transmittance spectra of the known chemical composition in the Sigma Library. Then we calculate the imaginary refractive index of that composition by determining both an effective sample thickness d_{eff} and a simple conversion factor C (C takes into account the surface reflection and internal scattering losses of the chemical powder in the composite medium and lumps as an effective absorption extinction) that match these values with published imaginary refractive-index values. The values of d_{eff} and C that would reproduce the already known imaginary refractive index of a known substance could be used as the representative values for the samples given in the Sigma Library of the measured transmission of radiation through the composite medium. The spectra in the Sigma Library were mostly made from samples prepared in the same manner as Nujol and were investigated with a similar experimental configuration.[22] Hence d_{eff} and C for the known composition will also represent d_{eff} of other not so well-known substances. For further mandatory confirmation, d_{eff} and C were also determined from a second well-known chemical composition, CAC, whose spectra were also given in the Sigma Library and that are similar to the one obtained for AMS. Hence, in this way, an estimate of d_{eff} and C for the uncharacterized chemical substance in the Sigma Library could be made that can then be used for the estimation of their k and n.

A. Imaginary Refractive Index

For FTIR measurements, the composite sample contains the chemical of interest dispersed in Nujol medium. For our study, the FTIR measurement is viewed as a composite dielectric medium of two compositions with effective thickness d_{eff}, and we assume that all scattering losses within the sample and reflection losses at all surfaces will be lumped into a single conversion factor C, where d_{eff} and C need to be determined. Then for incident intensity I_0 on the sample and intensity I after traversing distance d_{eff} through the thin composite sample, the transmittance $T(\lambda) = I/I_0$ at wavelength λ is given by[6]

$$T(\lambda) = [(1 - R)^2 \exp(-\alpha d_{\text{eff}})] / [1 - R^2 \exp(-2\alpha d_{\text{eff}})]. \quad (1)$$

Here α is the absorption coefficient of the composite sample given by $\alpha = 4\pi k/\lambda$ where k is the imaginary refractive index at λ of the chemical-in-Nujol composite and $R \equiv R(\lambda)$ is the surface reflectivity. For typical FTIR measurements with R small and $\alpha d_{\text{eff}} \sim 1$, the denominator of T does not differ much from 1 as

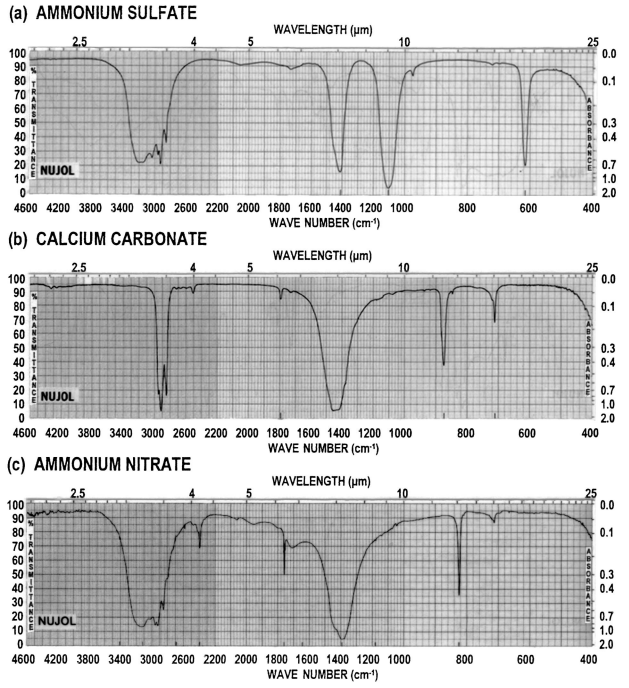

Fig. 1. FTIR absorbance and transmittance spectra from the Sigma Library[15] (reproduced with permission from Roger Keller) for (a) AMS, (b) CAC, (c) AMN.

the exponential term drops off quickly because of the square in the argument; therefore

$$T(\lambda) = C(\lambda)\,\exp(-\alpha d_{\text{eff}}), \quad \text{with } C(\lambda) = (1-R)^2 / [1 - R^2\exp(-2\alpha d_{\text{eff}})] \sim (1-R)^2, \quad (2)$$

where $C(\lambda)$ is the conversion factor taking into account any reflectivity losses at the surfaces and particulate scattering losses within the sample. As with $R(\lambda)$, $C(\lambda)$ is a function of λ; however, we assume here that it is constant within the FTIR measurement accuracy over the wavelength regime. It would be advantageous to have a complete set of measurements of $R(\lambda)$ for the dual-composite medium, but information on $R(\lambda)$ is not available in the Sigma Library. Therefore this simple first-order approximation was used for $C(\lambda)$ constant over the spectral range, which led to extremely good agreement with measurements, as we show below. Solving for k at a given measured T yields $k = -\lambda \ln(T/C)/4\pi d_{\text{eff}}$. If T and k are known for well-known compositions, then d_{eff} and C can be reliably determined. Once d_{eff} and C are known, then k can be easily determined from measured T for uncharacterized compositions.

AMS and CAC were chosen as the known compositions to determine d_{eff} and C because their spectra T are given in the Sigma Library and their complex refractive index[6,16] have been estimated. Figure 1 shows the three spectra from the Sigma Library[15] (reproduced here with permission from Roger Keller). The three chemical compositions all show quite similar baseline values, especially for higher wave numbers and for regions off the absorption peaks. Also, there are no observed indications of saturation by the strongest absorption peaks. Thus k can be determined for AMN if we assume d_{eff} and C are the same for all three samples, which, from the appearance of the FTIR data in Fig. 1, seems to be a valid assumption.

T was tabulated at nearly 120 values of wave number from the Sigma Library FTIR spectrum. Attention was given to the Nujol peaks occurring at 2914, 2856, 2724, 1461, 1377, and 722 cm^{-1} within the spectral band for the three spectra and were generally eliminated when we smoothed the measured T curves of the chemical composition when possible without losing the chemical's spectral information. For example, the combined Nujol peak at 2914 and 2856 cm^{-1}, shown clearly for CAC, was eliminated entirely, whereas these same peak locations were simply smoothed away for the AMS and AMN peaks because there was a peak associated with the chemical occurring near 3200 cm^{-1}. The two only slightly visible Nujol peaks occurring at 1461 and 1377 cm^{-1} were not smoothed out for they fell directly within the strong peak for AMS and AMN and would remain as a minor caveat to the absorption data. As for the 722-cm^{-1} peak, there is a slight indication of this peak in the AMS and hence was not smoothed out. This same peak is slightly larger for AMN, which has in addition a NO_3^- bending mode[13,14] at 722 cm^{-1}. This Nujol peak is most likely causing an additional resonance absorption in the same vicinity of the AMN resonance peak and thus was not smoothed out. This same Nujol peak is most likely hidden within the CAC peak[23] at 712.7 cm^{-1}.

An important step here is to establish the value for the unknown parameter d_{eff}. Using the tabulated T values for AMS and CAC, we used incremental values of d_{eff} of 0.7, 0.8, 1.0, 1.2, 1.4 μm in the equation for k until a best agreement for the whole wavelength regime was reached between k values from the FTIR spectral results and the corresponding published k data. Figure 2(a) shows the comparison for several incremental values of d_{eff} and for $C = 95$ for AMS, showing the sensitivity of k values to slight variations in d_{eff}. As shown in Fig. 2(a), a slight change in d_{eff} has an inconsequential effect on baseline values where there is little absorption in comparison with the peak values where absorption is much greater and the peak absorption k values are more affected by changes in d_{eff}. Therefore the best criterion to determine d_{eff} is to obtain the optimum agreement in the region of the peak absorption values. The value of $d_{\text{eff}} \sim 1.0$ μm gave the best overall agreement with the published k data for both AMS [as shown in Fig. 2(a)] and CAC.

We also examined the baseline of the T data by changing the value of C from 90 to 100 with $d_{\text{eff}} = 1.0$ μm, as shown in Fig. 2(b) for AMS data. The effect of changing C has more effect on the baseline values than the peak values, and still the effect on the baseline values is minimal as can be seen in Fig. 2(b). When the T spectra data are corrected by a factor C of 95, then the resulting k values for the baseline of

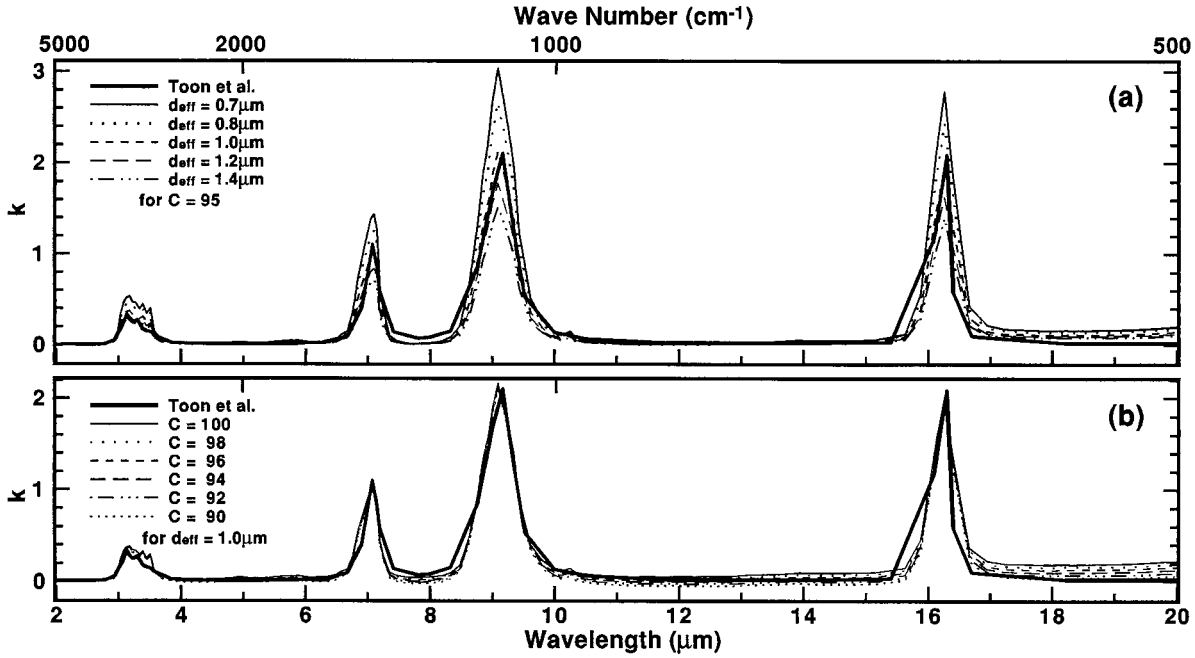

Fig. 2. Comparison of imaginary refractive index (Toon *et al.*[6]) k for AMS with calculated k from the Sigma FTIR data for the effect of changing the (a) effective composite thickness d_{eff}, (b) conversion factor C.

AMS, as shown in Fig. 2(b), agree remarkably well over the whole measured spectral range with the known published values. This value of $C = 95$ is also consistent with observation of the FTIR spectral data. For the three Sigma Library spectra (Fig. 1) in regions where there is almost negligible absorption with small k values, there is a residual T value of ~5% that was verified for the AMS, as shown in Fig. 2. The factor C accounts for probable losses in transmission that are due to consistent reflection losses at the surfaces and particulate scattering process losses within the sample. These terms are lumped as loss mechanisms because of the absorption extinction in Eq. (2), resulting in a bias in the T data that affects baseline values while having less effect on peak values. This confirms the need to correct T by C so we can use it for determining the k values of AMN.

Figure 3 shows calculated k as a function of λ for all three compositions from their respective FTIR spectra. For AMS [Fig. 3(a)] the comparison with Toon *et al.* data by use of transmittance measurements with a grown crystal sample is also presented,[6] showing excellent agreement within the spectral range. The slight discrepancy for a wave number smaller than 588 cm^{-1} (17 μm) in the FTIR spectra may be due to higher absorption in Nujol, giving rise to elevated k values. Nevertheless, detailed analysis would be needed to understand more fully the discrepancy in this spectral regime for both data sets. Likewise for CAC [Fig. 3(b)], the agreement of k from the FTIR data is also quite good with the data reproduced from Querry *et al.* by use of reflectance measurements of limestone samples taken from three different U.S. quarries.[16] In this case, the limestone data show elevated values of k for wave numbers smaller than 1333 cm^{-1} (7.5 μm), which was not explained by Querry *et al.* and may be due to the insensitivity of the reflectance measurement for small k in this spectral regime or perhaps impurities in the natural limestone giving enhanced reflectance. The determined k for AMN as shown in Fig. 3(c) is expected to be quite reasonable, on the basis of the detailed comparisons with AMS and CAC.

B. Real Refractive Index

The frequency-dependent imaginary and real refractive indices of a substance are integrally related. Thus $n(\nu)$ can be mathematically derived from $k(\nu)$ by use of a K–K transform. In its true form, the integral in this transform is computed over all frequencies. However, $k(\nu)$ in this study is known only over a finite set of frequencies ν, so a subtractive K–K transform must be applied[20,21]:

$$n(\nu) = n(\nu_0) + \frac{2(\nu^2 - {\nu_0}^2)}{\pi} \times P \int_{\nu_{\text{lo}}}^{\nu_{\text{hi}}} \frac{\nu' k(\nu')}{[\nu^2 - (\nu')^2][{\nu_0}^2 - (\nu')^2]}\, d\nu', \quad (3)$$

which is evaluated numerically. In Eq. (3) P signifies that the Cauchy principal value of the integral be taken, and $n(\nu_0)$ is a known value of the real refractive index at some frequency ν_0 within the integration limits ν_{lo} and ν_{hi} where k is small. This value of the real refractive index at ν_0, or the anchor point, is required so that all other values of $n(\nu)$ can be determined in relation to it, and it is determined from a separate measurement. These values are usually

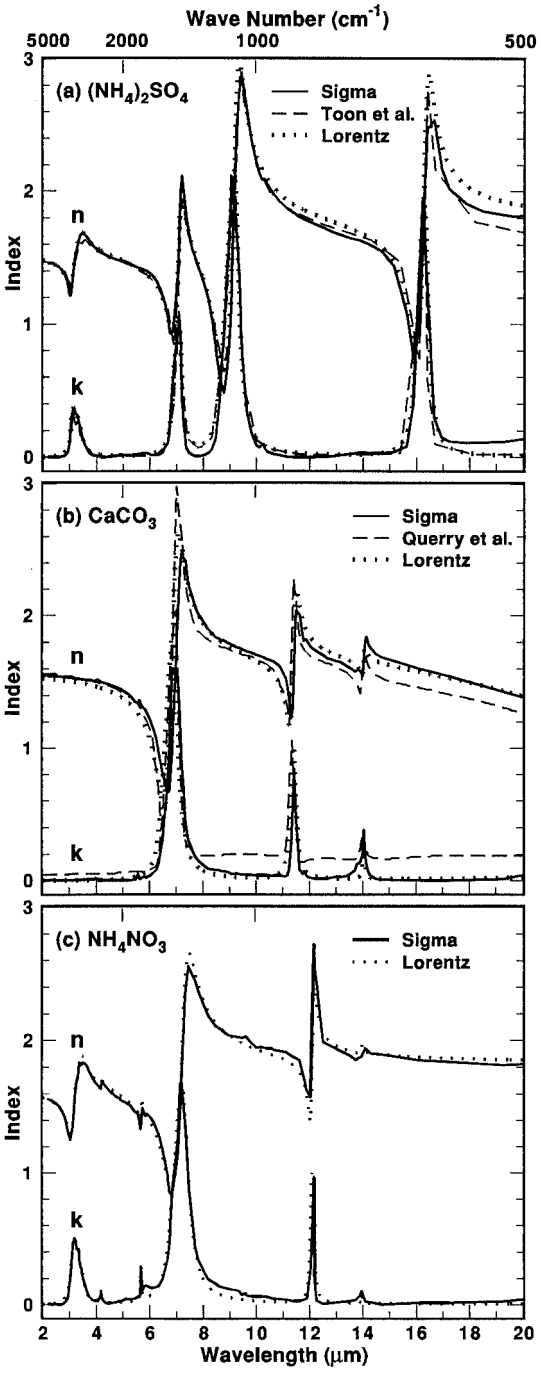

Fig. 3. Complex refractive index k as a function of wavelength for (a) AMS, (b) CAC, (c) AMN. The Toon *et al.* data are from Ref. 6. The Querry *et al.* data are from Ref. 16.

not available in the mid-IR, but are usually determined at shorter wavelengths.

The subtractive K–K determinations of n from the k data are also shown in Fig. 3. The comparisons for AMS and for CAC show excellent agreement. To perform the subtractive K–K calculations, the n values need an anchor point, which are AMS,[6] $n = 1.480$ at 2100 cm^{-1}; CAC,[24] $n = 1.559$ at 8100 cm^{-1} (average of the ordinary and extraordinary ray values); and AMN,[24] $n = 1.611$ at 17,000 cm^{-1} (He line, $\lambda = 0.5876$ μm). For AMS, a real index[6] at 2100 cm^{-1} was used in the mid-IR because it was available in the literature, and k is sufficiently small to justify that location and yet it does not go far enough toward the near IR where k is really zero. For AMN and CAC, we had to extend the k data to higher frequencies where the n values were known in the visible by setting all $k = 0$, assuming no significant absorption bands. For the subtractive K–K calculations, the extended values were kept with the data. We also extended the k values from 400 to 0 cm^{-1} by setting all $k = k$ at 400 cm^{-1} to minimize truncation effects in the K–K calculation. These artificial index values were trimmed from the final data sets.

It was found that for a wave number less than 500 cm^{-1} discrepancies in n occurred that are related to the initial k values. The FTIR spectral data from 500 to 400 cm^{-1} show that k increases rapidly beyond 500 cm^{-1}. Such spectral behavior could be attributed to actual chemical absorption itself or possibly affected by Nujol absorption or slight detector insensitivity at the longest wavelengths. Nevertheless, because of the way k is estimated to 0 cm^{-1}, the unexpected rapid increase in k beyond 500 cm^{-1} causes its corresponding n to decrease more rapidly. For AMS, the two data sets are in much better agreement in n, particularly at less than 1000 cm^{-1}, after the truncation of the k data is performed at 500 cm^{-1} rather than at 400 cm^{-1} and then when the subtractive K–K transform is recalculated. Without truncation of the k data, there is an even greater departure from agreement. However, for CAC, trimming the data at 500 cm^{-1} gave worse agreement; henceforth, the data were not trimmed off prior to the calculations. In this case, however, the rise in absorption beyond 500 cm^{-1} may contain some measurement artifacts. This rise in absorption is also in part due to the effect of a stronger CAC absorption peak near 300 cm^{-1}, which affects these measurements at the longer wave numbers.[23] As for AMN, both AMS and AMN show similar absorption structure in the far IR beyond 500 cm^{-1}. AMN has no peak[13,14] from ~700 to 300 cm^{-1}, and AMS begins to have structure further out in wave numbers beyond 200 cm^{-1}. Because trimming the data for AMS gave better agreement and because AMN lacks structure in the far IR, the data were trimmed for AMN beyond 500 cm^{-1} for the subtractive K–K analysis. Table 1 shows the tabulated k and n values for AMN as shown in Fig. 3(c). These tabulated complex refractive indices are thus a continuation and in agreement of earlier published values[25] for the wavelength regime from 0.7 to 2.6 μm.

Depending on the quality of the FTIR data at the shorter wave-number regime, trimming the spectral data may be necessary to give the most reliable data for k, and consequently for n, by use of the subtractive K–K analysis. The shorter wavenumber region of FTIR spectral data is most in question because of Nujol absorption and possible slight detector insensitivities, so it is imperative to

Table 1. Optical Constants of Ammonium Nitrate

ν (cm^{-1})	λ (μm)	n	k
4600	2.17	1.56	2.75×10^{-3}
4500	2.22	1.55	5.67×10^{-3}
4400	2.27	1.55	1.91×10^{-3}
4340	2.30	1.55	5.88×10^{-3}
4300	2.33	1.55	1.96×10^{-3}
4200	2.38	1.54	1.00×10^{-3}
4100	2.44	1.53	3.09×10^{-3}
4000	2.50	1.53	3.17×10^{-3}
3900	2.56	1.51	0.00×10^{0}
3800	2.63	1.50	8.84×10^{-4}
3700	2.70	1.48	1.13×10^{-3}
3600	2.78	1.44	9.51×10^{-3}
3500	2.86	1.40	2.40×10^{-2}
3400	2.94	1.31	5.53×10^{-2}
3300	3.03	1.25	2.09×10^{-1}
3200	3.12	1.35	4.59×10^{-1}
3121	3.20	1.55	5.07×10^{-1}
3080	3.25	1.66	4.77×10^{-1}
3060	3.27	1.69	4.18×10^{-1}
3010	3.32	1.72	4.25×10^{-1}
2980	3.36	1.81	4.16×10^{-1}
2970	3.37	1.83	3.58×10^{-1}
2950	3.39	1.82	3.11×10^{-1}
2915	3.43	1.81	2.80×10^{-1}
2900	3.45	1.82	2.74×10^{-1}
2882	3.47	1.83	2.39×10^{-1}
2850	3.51	1.83	2.09×10^{-1}
2820	3.55	1.83	1.70×10^{-1}
2800	3.57	1.82	1.50×10^{-1}
2770	3.61	1.82	1.23×10^{-1}
2750	3.64	1.81	1.01×10^{-1}
2700	3.70	1.78	6.58×10^{-2}
2650	3.77	1.75	5.16×10^{-2}
2580	3.88	1.71	3.43×10^{-2}
2520	3.97	1.68	2.78×10^{-2}
2510	3.98	1.68	2.79×10^{-2}
2480	4.03	1.67	3.57×10^{-2}
2460	4.07	1.66	3.41×10^{-2}
2415	4.14	1.64	5.66×10^{-2}
2400	4.17	1.64	7.40×10^{-2}
2395	4.18	1.64	1.04×10^{-1}
2380	4.20	1.70	5.75×10^{-2}
2350	4.26	1.68	2.98×10^{-2}
2320	4.31	1.66	1.85×10^{-2}
2280	4.39	1.65	1.12×10^{-2}
2200	4.55	1.61	1.08×10^{-2}
2090	4.78	1.57	2.06×10^{-2}
2061	4.85	1.57	2.74×10^{-2}
2040	4.90	1.56	2.11×10^{-2}
2020	4.95	1.55	2.57×10^{-2}
1957	5.11	1.53	4.33×10^{-2}
1940	5.15	1.53	4.37×10^{-2}
1900	5.26	1.51	3.93×10^{-2}
1830	5.46	1.46	4.84×10^{-2}
1800	5.56	1.44	6.13×10^{-2}
1780	5.62	1.38	6.20×10^{-2}
1770	5.65	1.33	7.73×10^{-2}
1760	5.68	1.35	2.90×10^{-1}
1745	5.73	1.49	1.08×10^{-1}
1725	5.80	1.45	1.41×10^{-1}
1710	5.85	1.43	1.45×10^{-1}
1690	5.92	1.44	1.44×10^{-1}
1660	6.02	1.42	1.30×10^{-1}
1630	6.13	1.39	1.29×10^{-1}
1600	6.25	1.33	1.34×10^{-1}
1570	6.37	1.27	1.55×10^{-1}
1540	6.49	1.17	2.00×10^{-1}
1500	6.67	1.00	3.40×10^{-1}
1480	6.76	0.85	4.65×10^{-1}
1460	6.85	0.84	8.49×10^{-1}
1430	6.99	1.05	1.17×10^{0}
1420	7.04	1.16	1.26×10^{0}
1400	7.14	1.50	1.67×10^{0}
1395	7.17	1.64	1.68×10^{0}
1390	7.19	1.77	1.69×10^{0}
1362	7.34	2.38	1.31×10^{0}
1341	7.46	2.56	9.25×10^{-1}
1300	7.69	2.45	4.57×10^{-1}
1280	7.81	2.37	3.40×10^{-1}
1220	8.20	2.18	1.94×10^{-1}
1180	8.47	2.11	1.59×10^{-1}
1160	8.62	2.09	1.40×10^{-1}
1120	8.93	2.04	1.22×10^{-1}
1099	9.10	2.03	1.15×10^{-1}
1070	9.35	2.02	1.05×10^{-1}
1058	9.45	2.02	7.49×10^{-2}
1042	9.60	2.03	8.94×10^{-2}
1040	9.62	2.02	7.17×10^{-2}
1020	9.80	1.98	6.42×10^{-2}
1000	10.00	1.95	6.36×10^{-2}
980	10.20	1.95	6.49×10^{-2}
960	10.42	1.94	6.16×10^{-2}
943	10.60	1.94	4.84×10^{-2}
938	10.66	1.93	4.59×10^{-2}
900	11.11	1.91	3.80×10^{-2}
880	11.36	1.88	2.70×10^{-2}
860	11.63	1.85	2.77×10^{-2}
840	11.90	1.62	5.12×10^{-2}
830	12.05	1.57	2.59×10^{-1}
822	12.16	2.72	9.66×10^{-1}
820	12.20	2.54	1.67×10^{-1}
817	12.24	2.46	3.13×10^{-2}
800	12.50	1.98	5.25×10^{-3}
740	13.51	1.89	2.87×10^{-2}
728	13.74	1.85	3.51×10^{-2}
720	13.89	1.87	7.21×10^{-2}
717	13.95	1.88	1.04×10^{-1}
710	14.08	1.94	2.38×10^{-2}
700	14.29	1.90	1.81×10^{-2}
680	14.71	1.89	0.00×10^{0}
620	16.13	1.85	1.36×10^{-2}
580	17.24	1.84	1.45×10^{-2}
520	19.23	1.81	2.44×10^{-2}
500	20.00	1.82	4.24×10^{-2}

understand the measurements as well as know the spurious peaks in the spectra, such as those that are due to Nujol. Estimating k is not simple by any method; and because of its frequency dependence, any errors in the absorption data that are due to improper scaling will manifest as larger errors in k at the lower frequencies. Consequently, it is always best to eliminate uncertainties at the lower frequencies before one performs subtractive K–K analysis.

Table 2. Lorentz Parameters Calculated for Absorbance and Transmittance Spectral Data

j	λ_j	ν_j	ρ_j	γ_j
Ammonium Sulfate, $\varepsilon_\infty = 2.29$				
1	3.18	3140.0	0.00900	0.1000
2	4.88	2050.0	0.00020	0.0521
3	5.88	1700.0	0.00002	0.0080
4	7.07	1415.0	0.00850	0.0350
5	11.45	873.0	0.03400	0.0440
6	14.04	712.4	0.01400	0.0200
Calcium Carbonate, $\varepsilon_\infty = 2.38$				
1	7.02	1425.0	0.0320	0.0521
2	11.45	873.0	0.0055	0.0188
3	14.04	712.4	0.0004	0.0070
4	33.00	303.0	0.1400	0.0620
Ammonium Nitrate, $\varepsilon_\infty = 2.62$				
1	3.23	3100.0	0.01300	0.1000
2	4.18	2394.0	0.00020	0.0100
3	5.69	1758.0	0.00040	0.0080
4	7.31	1368.0	0.03800	0.0680
5	12.12	825.0	0.00350	0.0110
6	13.95	717.0	0.00007	0.0020

3. Lorentz Dispersion Theory

We also determined the complex refractive index from the FTIR spectra using classical Lorentz dispersion theory.[6] The complex dielectric function $\varepsilon(\lambda)$ is related to $n(\lambda)$ and $k(\lambda)$ as $\varepsilon(\lambda) = [n(\lambda) + ik(\lambda)]^2$. From the dispersion theory, $\varepsilon(\nu)$ at wave number $\nu = \lambda^{-1}$ is expressed as

$$\varepsilon(\nu) = \varepsilon_\infty + \sum_j \frac{4\pi\rho_j\nu_j^2[(\nu_j^2 - \nu^2) + i\gamma_j\nu_j\nu]}{(\nu_j^2 - \nu^2)^2 + (\gamma_j\nu_j\nu)^2}, \quad (4)$$

where ε_∞ is the high-frequency dielectric constant and the three Lorentz parameters of the jth IR active band are given by $\nu_j = \lambda_j^{-1}$ that is the central wavenumber position (not to be confused with frequency ν), ρ_j is the strength, and γ_j is the damping coefficient. So use of this method, knowledge of the peak location, its strength, and its width are necessary for this series computation. Shown also in Fig. 3 are the complex refractive-index values for AMS, CAC, and AMN computed with the Lorentz dispersion theory. Table 2 shows the Lorentz parameters to determine the $n(\lambda)$ and $k(\lambda)$ for each of the three compositions. We obtained the parameters by simultaneously matching the calculated $n(\lambda)$ and $k(\lambda)$ with the derived complex refractive-index values from the FTIR spectral data. The ε_∞ (shown in Table 2) were adjusted freely to match the baseline of the Lorentz dispersion theory calculations with the derived values from the FTIR spectral data. The measured n values[24] for higher frequencies are $n \sim 1.482$ (Na line, $\lambda = 0.5893$ μm) for AMS; $n = 1.559$ ($\lambda = 1.229$ μm) for CAC; $n = 1.611$ (He line, $\lambda = 0.5876$ μm) for AMN and with $k \sim 0$. With $\varepsilon_\infty \sim n^2$, the n^2 values of 2.20 for AMS, 2.43 for CAC, and 2.59 for AMN compare with excellent agreement with these freely adjusted ε_∞ values (given in Table 2) with an accuracy of 4.09%, 2.06%, and 1.16%, respectively. Note that implicit in these calculations is d_{eff} because the thickness directly affects peak absorbance. The comparison of $n(\lambda)$ and $k(\lambda)$ from the Lorentz dispersion theory is in excellent agreement, even in the regions of resonance having strong anomalous dispersion. The emphasis in this theoretical exercise is to reinforce the fact that, if the three parameters for each resonant absorption peak could be reliably constructed from FTIR spectra or known from first principles of molecular physics, the complex refractive index as a function of wavelength for chemical compositions could be reliably determined with the classical Lorentz dispersion theory.

4. Backscatter Calculations

AMN and AMS aerosols are commonly found in the atmosphere mostly from anthropogenic sources. One such area on the Earth where both types of aerosol are prevalent is over the San Joaquin Valley in California and the surrounding nearby areas.[17,18] This is a large agricultural region of the western United States having both rural and urban contributions. Combined with automobile exhaust pollution and the effects of population growth, it is considered a significant region for anthropogenically produced aerosols contributing to the $PM_{2.5}$ declared important by the U.S. Environmental Protection Agency for affecting human life in terms of visibility, pollution, and health effects. For anthropogenic aerosols with sulfur dioxide and nitrous oxide competing for ammoniation, AMN aerosol chemistry is closely linked[19] with AMS aerosol chemistry, the latter being important for climate forcing.[1,2] Hence it is important to distinguish between the two in urban–rural-type regions.

A comparison of backscatter coefficient β measurements from two cw CO_2 Doppler lidars operating at 9.1- and 10.6-μm wavelengths with β modeling by use of measured aerosol size distributions[26] during an airborne National Aeronautics and Space Administration (NASA) mission in California show that AMN, as an important atmospheric constituent in the San Joaquin region, necessitates its incorporation in any effort to model aerosol scattering for that particular region and may be relevant for other such rural–urban regions. To model the wavelength-dependent β, the complex refractive index for AMN is needed at various wavelengths. Knowing the signature of AMN, in the IR refractive index and backscatter, will help to remotely detect its presence with a single multiwavelength lidar spectrometer being developed at NASA, an instrument to be used to determine aerosol composition with the retrieved wavelength-dependent β signal.

To show the effect of the complex refractive index on electromagnetic scattering, β calculations were performed for AMN and AMS between a 2- and 20-μm wavelength range as shown in Fig. 4. This comparison illustrates the differences in expected β for the two atmospheric aerosols having their differing optical properties. We similarly performed[27] the calculations using a log-normal size distribution with

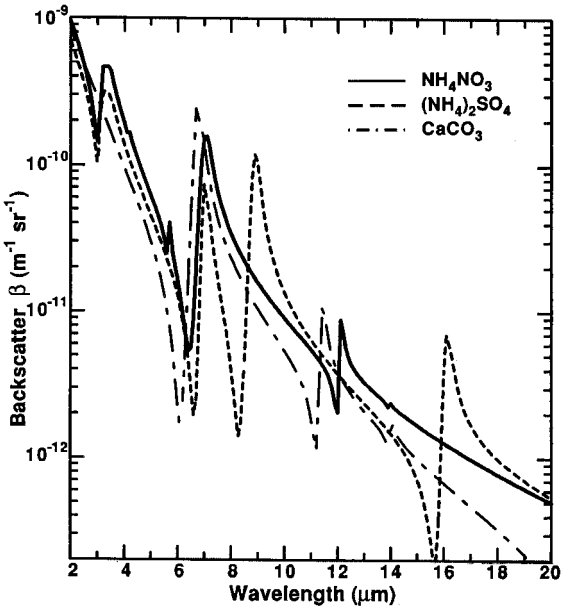

Fig. 4. Calculated backscatter coefficient β as a function of wavelength λ for log-normal size distribution having N_0 = 1 particle/cm^3, r_g = 0.15 μm, and δ_g = 1.5 by use of the complex refractive-index values from the Lorentz dispersion theory as shown in Fig. 3 for AMS, CAC, and AMN.

mode radius r_g = 0.15 μm and a geometric standard deviation σ_g = 1.5. β varies by over 3 orders of magnitude within this designated wavelength range, showing the greatest effect near the absorption resonance peaks. For wavelengths shorter than ~7 μm and longer than 18 μm, β is quite equivalent; however, between 7 and 18 μm there are the specific peaks showing the characteristic signature of the compositions with β varying dramatically. These results suggest that an instrument, like a lidar, measuring β between a 7- and 18-μm wavelength could distinguish the relative abundance of each composition in atmospheric aerosols when specifically selected wavelengths are used that correspond to on and off peaks for each chemical composition. Therefore, within the extended CO_2 band between 9 and 12 μm, a computer-controlled wavelength-tunable CO_2 Doppler lidar could infer aerosol compositional information composed mostly of these two chemical compositions. In this CO_2 wavelength range, nature offers the large resonance for AMS, peaking near 9.1 μm whereas AMN shows no resonance here with only a slight decrease in β with increasing wavelength. Hence, at this wavelength, β for AMS aerosol would be close to an order of magnitude greater than that for pure AMN. However, at 10.6-μm wavelength, β for both compositions are nearly equal, offering an off-peak wavelength reference point. This comparison illustrates that AMN has little structure in the CO_2 wavelength band that makes it possible to distinguish it from AMS in an atmospheric aerosol. Just as in the visible and near IR, the absorption lines of gases can be used to distinguish them by the differential absorption lidar method, known also as DIAL, so in the CO_2 IR, the signature of β may help distinguish several aerosol compositions.

As a further comparison with the AMN and AMS β values, β for CAC is also shown in Fig. 4. Although CAC is not a prevalent aerosol in the atmosphere, except perhaps near limestone quarries, this comparison further illustrates the complexity of expected β for another chemical substance as depicted by the absorption peak structure in Fig. 1. The three absorption peaks of CAC are observed; however, the peak near 14 μm is barely evident after the β calculations. At short wavelengths, all three β values converge in the Rayleigh limit, as expected, whereas at higher wavelengths CAC overall tends to have weaker β values because of its smaller real part.

5. Conclusion

Because aerosol types can vary with location, it is becoming more obvious that, to understand the effect of atmospheric aerosols on global climate forcing, their compositions and thus their complex refractive index need to be known. Nitrates are important atmospheric aerosol constituents but not all their properties are known, which led to a methodology to determine the complex refractive index for AMN in the 2–20-μm spectral range from the earlier published high-quality FTIR absorbance and transmittance spectrum in the Sigma Library data set.[15] Use was made of the FTIR spectra for AMS and CAC found in the same data set where the k and n values derived from the FTIR spectra were compared with their rigorously determined complex refractive index from previously published sources. From this comparison for AMS and CAC and with a simplified equation for transmittance, we obtained the unknown sample effective thickness d_{eff} and the conversion factor C inferred from this equation to determine the unknown complex refractive index for AMN, also from the available FTIR spectra. The results thus show that, by use of the simplified equation and lumping reflection and scattering extinction with absorption extinction in the simplified equation, we can obtain excellent comparison with those rigorously derived values by earlier investigators. Other compositions for which FTIR spectra are available can be similarly converted to their complex refractive index, provided that all the necessary parameters are either available with the spectra or can be inferred by comparison. This simple technique allows the inference and excellent estimation of optical properties from the many previously existing FTIR-type data sets, even though they were designed for other applications, because measuring high-quality spectra for the required compositions is not always possible.

This research was performed under National Aeronautics and Space Administration (NASA) cooperative agreement NCC8-142 and NCC8-200. The research of K. A. Fuller was supported by the NASA Global Aerosol Climatology Project, grant NCC8-200. The authors thank Ramesh Kakar, NASA Headquarters Office of Earth Science, for his support and

Krishnan Chittur, University of Alabama at Huntsville, for helpful discussions.

References

1. R. J. Charlson, S. E. Schwartz, J. M. Hales, R. D. Cess, J. A. Coakley, J. E. Hansen, and D. J. Hofmann, "Climate forcing by anthropogenic aerosols," Science **255,** 423–430 (1992).
2. R. J. Charlson and T. M. L. Wigley, "Sulfate aerosol and climatic change," Sci. Am. **270,** 48–57 (1994).
3. W. M. Irvine and J. B. Pollack, "Infrared optical properties of water and ice spheres," Icarus **8,** 324–360 (1968).
4. K. F. Palmer and D. Williams, "Optical constants of sulfuric acid: application to Venus?" Appl. Opt. **14,** 208–219 (1975).
5. L. J. Richwine, M. L. Clapp, and R. E. Miller, "Complex refractive indices in the infrared of nitric acid trihydrate aerosols," Geophys. Res. Lett. **22,** 2625–2628 (1995).
6. O. B. Toon, J. B. Pollack, and B. N. Khare, "The optical constants of several atmospheric aerosol species: ammonium sulfate, ammonium oxide, and sodium chloride," J. Geophys. Res. **81,** 5733–5748 (1976).
7. F. E. Volz, "Infrared optical constants of ammonium sulfate, Sahara dust, vocanic pumice, and flyash," Appl. Opt. **12,** 564–568 (1973).
8. J. B. Pollack, O. B. Owen, and B. N. Khare, "Optical properties of some terrestrial rocks and glasses," Icarus **19,** 372–389 (1973).
9. O. Toon, J. B. Pollack, and C. Sagan, "Physical properties of the particles composing the Martian dust storm of 1971–1972," Icarus **30,** 663–696 (1977).
10. D. P. Walter, D. E. Cooper, J. E. van der Laan, and E. R. Murray, "Carbon dioxide laser backscatter signature from laboratory generated dust," Appl. Opt. **25,** 2506–2513 (1986).
11. T. Roush, J. Pollack, and J. Orenberg, "Derivation of midinfrared (5–25 μm) optical constants of some silicates and palagonite," Icarus **94,** 191–208 (1991).
12. A. Ben-David, "Wavelength dependence of backscattering and extinction of kaolin dust at CO_2 laser wavelengths: effect of multiple scattering," Appl. Opt. **32,** 1598–1605 (1993).
13. F. F. Bentley, L. D. Smithson, and A. L. Rozek, *Infrared Spectra and Characteristic Frequencies ~700-300 cm^{-1}: A Collection of Spectra Interpretation and Bibliography* (Interscience, New York, 1968).
14. K. Nakamoto, *Infrared Spectra of Inorganic and Coordination Compounds* (Wiley-Interscience, New York, 1970).
15. R. J. Keller, *Sigma Library of FT-IR Spectra* (Sigma Chemical Company, St. Louis, Mo., 1986), Vol. 1.
16. M. R. Querry, G. Osborne, K. Lies, R. Jordan, and R. M. Coveney, Jr., "Complex refractive index of limestone in the visible and infrared," Appl. Opt. **17,** 353–356 (1978).
17. J. C. Chow, J. G. Watson, D. H. Lowenthal, P. A. Solomon, K. L. Magliano, S. D. Ziman, and L. W. Richards, "PM 10 source apportionment in California's San Joaquin Valley," Atmos. Environ. Part A **26,** 3335–3354 (1992).
18. J. C. Chow, J. G. Watson, D. H. Lowenthal, P. A. Solomon, K. L. Magliano, S. D. Ziman, and L. W. Richards, "PM10 and PM2.5 compositions in California's San Joaquin Valley," Aerosol Sci. Technol. **18,** 105–128 (1993).
19. U.S. Environmental Protection Agency, *Air Quality Criteria for Particulate Matter*, National Center for Environmental Assessment Office of Research and Development, EPA/600/P-95/001aF (U.S. Environmental Protection Agency, Research Triangle, N. C., 1996), Vol. 1, pp. 6-163–6-168.
20. K. F. Palmer, B. E. Wood, and J. A. Roux, "Infrared optical properties of solid mixtures of molecular species at 20 K," AEDC-TR-80-30 (Arnold Engineering Development Center, Arnold Air Force Base, Tenn., 1981).
21. M. L. Clapp, D. R. Worsnop, and R. E. Miller, "Frequency dependent optical constants of water ice obtained directly from aerosol extinction spectra," J. Phys. Chem. **99,** 6317–6326 (1995).
22. R. J. Keller, Sigma Chemical Company, 3050 Spruce Street, St. Louis, Missouri 63103 (personal communication, 2000–2002).
23. W. J. Tropf, "Calcium carbonate, calcite ($CaCO_3$)," in *Handbook of Optical Constants of Solids III*, (Academic, New York, 1998).
24. R. C. Weast, ed., *CRC Handbook of Chemistry and Physics*, 58th ed. (CRC Press, New York, 1971), pp. E-219 and E-223.
25. S. F. Gosse, M. Wang, D. Labrie, and P. Chylek, "Imaginary part of the refractive index of sulfates and nitrates in the 0.7–2.6-μm spectral region," Appl. Opt. **36,** 3622–3634 (1997).
26. D. R. Cutten, M. A. Jarzembski, V. Srivastava, R. F. Pueschel, S. D. Howard, and E. W. McCaul, Jr., "Boundary layer aerosol composition over Sierra Nevada Mountains using 9.11- and 10.59-μm cw lidars and modeled backscatter from size distribution data," J. Geophys. Res. (to be published) (2002).
27. V. Srivastava, M. Jarzembski, and D. A. Bowdle, "Comparison of calculated aerosol backscatter at 9.1- and 2.1-m wavelengths," Appl. Opt. **31,** 1904–1906 (1992).